https://dx.doi.org/10.1016/j.istruc.2019.01.023

Concentrated-plasticity modelling of circular concrete-filled steel tubular members under flexure

Yadong Jiang[1,2], António Silva[1,2], Luís Macedo[2], José Miguel Castro[2*], Ricardo Monteiro[1] and Tak-Ming Chan[3]

[1] Universitario di Studi Superiori di Pavia, Italy
[2] Faculty of Engineering, University of Porto, Portugal
[3] Department of Civil and Environmental Engineering, The Hong Kong Polytechnic University, Hong Kong
*corresponding author, e-mail address: miguel.castro@fe.up.pt

Abstract:

The research reported herein aims at the proposal of an accurate and efficient simplified numerical modelling approach for circular Concrete-Filled Steel Tubular (CFST) members under flexural loading. Experimental tests were carried out to characterize the bending behaviour of CFST members under monotonic and cyclic loading. The observed behaviour was characterized by strength and stiffness deterioration effects, as a result of the development of local buckling of the steel tube and cracking of the concrete core. Numerical simulations of these tests were conducted by resorting to existing modelling approaches, namely through Distributed Plasticity (DP) and Concentrated Plasticity (CP) models. It was found that existing modelling approaches failed to accurately capture the levels of strength deterioration and pinching effects observed in the tests. Thus, a novel CP-based simplified model, designated by *matCFSTdet*, was implemented in OpenSees. The hysteretic response of the CP model is based on a novel rotational spring model. An advanced calibration framework was introduced with targets to calibrate the accuracy of the model. The validation analyses indicate that the model is able to capture well the deterioration in both strength and stiffness of CFST members under cyclic flexural loading. Furthermore, the elastic stiffness, ultimate strength and the pinching effects of the hysteretic loops were also well simulated. The proposed CP model, coupled with the advanced calibration framework, thus results in a more realistic simulation of the cyclic flexural response of circular CFST members.

Keywords: *concrete-filled steel tube, concentrated plasticity model, OpenSees, experimental test*

1. Introduction

In recent years, concrete-filled steel tubes (CFST) have been increasingly used in seismic areas. The composite effect associated with these members, resulting from the interaction between the concrete core and the steel tube, can benefit both the member's capacity and ductility. This is, in part, a consequence of the confinement stress provided by the encasing tube to the concrete core. This confinement effect is generally more significant in comparison to reinforced concrete members, since the concrete section is fully encased by the steel tube. Furthermore, concrete cracking is delayed which improves the ductility of the concrete material. Reciprocally, the steel tube is constrained from buckling to the internal side of the cross-section, which improves the ductility of the tube. All these characteristics are very advantageous in a seismic context.

To evaluate the seismic performance of a composite structure with CFST members, reliable numerical modelling techniques are crucial. Two approaches are often adopted for the simplified modelling of CFST members, namely a Distributed Plasticity (DP) approach and a Concentrated Plasticity (CP) approach. In the DP approach, the CFST cross-section is simplified as a fibre section, with material properties assigned separately. Several research studies have been conducted with the use of fibre-discretized sections to simulate the flexural response of circular CFSTs under monotonic [1,2] and cyclic loading [3–6]. One drawback of using this approach is the inability to capture local buckling of the steel tube. A number of authors neglect this aspect by considering that the physical presence of the concrete core can reduce the influence of local buckling of the steel tube on the member's ductility [1,4–6]. According to [2] , the steel material constitutive law under compression and tension should be considered separately, with no hardening for the former. On the other hand, other research studies [7–9], have adopted a critical strain value as the trigger to the occurrence of local buckling. This parameter was found to be related to the CFST's cross-section slenderness. For rectangular CFST members, a number of researchers [10,11] have defined an ineffective area on the fibre section to represent the local buckling effect. This methodology has yet to be extended to the modelling of circular CFST members. In comparison to the DP models, CP models seem to be less widespread across the relevant literature. The authors of [14] and [6] derived analytical hysteretic rules for rectangular CFST sections and circular CFST sections, respectively. These formulations were used to characterise nonlinear rotational springs, but no further studies were carried out to embed the spring model into Finite Element (FE) software applications. The authors of [15] employed the *ModIMKPeakOriented* material model [16] that

is implemented in OpenSees [17], whilst [18] also utilized the *ModIMKPeakOriented* model as the rotational spring of CP model for seismic performance assessment of composite frames.

This research paper focuses on the proposal of a simplified model for CFST members with a Concentrated Plasticity approach. Monotonic and cyclic experimental responses of circular CFST member under flexural loading are considered to evaluate the accuracy of the existing DP and CP models for CFST members. A novel rotational spring model, which aims at a more realistic representation of the hysteretic behaviour of circular CFSTs, is developed through an advanced model calibration framework. This model is calibrated and validated against the experimental tests considered herein, showing significant improvements of simulated member responses in comparison to the existing DP and CP models available in the literature.

2. Experimental tests

To characterize the monotonic and cyclic bending behaviour of circular CFST columns, several experimental tests were conducted by the authors [19]. Table 1 lists the details associated with the 16 CFST specimens considered in this experimental campaign. It should be noted that the tested specimen list contains both Rubberised Concrete CFSTs (RuCFST) and conventional CFST members. Since the authors [19] showed that the use of rubberized concrete mixtures has no implications on the monotonic and cyclic flexural responses of the members, the RuCFST specimens are treated as normal CFST in this research. The following sections summarize the main experimental findings observed.

2.1 Test observations

Testing was conducted until the maximum displacement of the actuator was reached. The actuator ranges are between ± 150 mm for tests without constant axial load, and between ± 70 mm for tests with constant axial load. During testing, the specimens No.9, No.11, No.13 and No.15 were observed to have steel fracture occurred at the local buckling locations. The influence of cyclic loading on the flexural capacity of CFST member was studied by comparing the bending response of specimens under monotonic loading (specimen No.1 ~ No.8) and cyclic loading (specimens No.9 ~ No.16). Generally, in the monotonic and cyclic tests, all specimens developed local buckling in the plastic hinge region. Since this research aims to study the cross-sectional behaviour of CFST members, the test results are plotted in form of bending moment and drift ratio, the latter defined as the ratio between lateral displacement and the specimen's test length (1.35m). In Figure 1, each plot compares the monotonic and cyclic response of two specimens with the same characteristics, namely the same external diameter,

steel tube thickness, concrete/steel properties and constant axial load. The fracture points of four specimens, which had steel fracture occurred, are highlighted with red markers.

Analysis of the results shown in Figure 1 allows concluding that, for monotonic lateral loading, little to no strength degradation was observed in the tests, even for high levels of lateral deformation, in which local buckling of the steel tube was clearly visible. This indicated that the CFST specimen exhibited ductile behaviour under monotonic loading, as the concrete core delayed the occurrence of local buckling and minimized its influence on the response. Regarding the cyclic behaviour, significant strength deterioration was observed, which was mainly due to the continuous development of local buckling at the plastic hinge region, which even led to the fracture of steel tube (specimen No.9, No.11, No.13 and No.15). Therefore, the cyclic response of CFST members is generally more sensitive to this phenomenon, in comparison to monotonic loading. Moreover, some pinching effects were also observed in the response, suggesting that the opening and closing of the concrete cracks within the concrete core also influenced the member's overall response.

2.2 Monotonic and cyclic behaviour

The test results of specimen No.3 (monotonic loading) and No.11 (cyclic loading) are taken as examples to illustrate the bending response of circular CFST members. Regarding the monotonic flexural behaviour, as shown in Figure 2, the monotonic curve of circular CFST member can be separated into three stages. Segment *OA* in the figure represents the linear elastic stage of the response. In this stage, whilst concrete cracking could develop under tensile stresses, due to the low contribution of the concrete tensile strength to the member bending capacity, the response of CFST member behaviour can be considered linear. Segment *AB* represents the transition stage of the CFST, in which the steel tube cross-section is partially plastic. The *BC* segment represents the post-yield stage where the entire cross-section behaves inelastically. The CFST's bending behaviour in this stage involves multiple mechanisms, namely concrete crushing, concrete confinement effects and steel tube local buckling effects.

Regarding the cyclic behaviour of circular CFSTs, one cycle with drift ratio level around 4%, cycle *p* ($p_1p_2p_3$), and one cycle with drift ratio level around 9%, cycle *q* ($q_1q_2q_3q_4q_5$), are marked and compared, as shown in Figure 2. The bending capacity of cycle *q* is significantly lower than that of cycle *p*, which further proves the presence of strength degradation. It can be observed that, for the two cycles, their endpoints (p_1 and q_1) have lower moment values than their start points (p_3 and q_5), which indicates that the strength deterioration is related to the

accumulated deformation not the absolute deformation. Besides the deterioration on strength, the unloading stiffness of cycle *q* is lower than one of cycle *p*, which evidences that the stiffness deterioration is also related to the accumulated deformation. Figure 3 shows an idealized diagram of concrete cracking. Under large deformations, a concrete crack develops at the root region of CFST member. The unloading curve q_1q_2 (or q_3q_4) of Figure 2 results from the opening of this crack, as shown in Figure 3 (a). Portion q_2q_3 (or q_4q_5) of Figure 2, which is caused by the re-contact of concrete crack, is corresponding to the conditions shown in Figure 3 (b) and (c). Due to the opening and closing of the concrete crack, a pinching effect in the hysteretic response is generated. Considering the fact that there is a pinching effect on cycle *q* but not on cycle *p*, it can be concluded that the pinching effect is developing with the increase of accumulated displacement. It should be highlighted that Figure 3 shows an ideal developed concrete crack, which is symmetric. In reality, the concrete cracks may not be symmetrically developed, which entails asymmetric hysteretic loops as shown for specimen No.9.

3. Numerical modelling approaches of CFSTs members under flexure

For the purpose of seismic performance assessment of composite structures, simplified numerical models for the simulation of CFST members is essential. This stems from the computational demand associated with conducting many time-history analyses of structures (e.g. buildings, frames) in a more detailed fashion (e.g. full 3D finite element numerical model). As briefly discussed in Section 1 of this paper, two alternative simplified modelling approaches are generally employed in the literature, namely: i) Distributed Plasticity (DP) (Figure 4 left), and ii) Concentrated Plasticity (CP) (Figure 4 right). In this section, the advantages and drawbacks of the existing simplified models for CFST members are discussed. A newly developed lumped-plasticity rotational spring model, which aims to more accurately simulate the flexural behaviour of circular CFSTs, is detailed.

3.1 Existing simplified CFST models

3.1.1 Distributed plasticity

DP models are commonly adopted in the literature [1,3,6,7,14,20–23] in the context of monotonic and cyclic flexural response of circular CFST. As shown in Figure 4 (left), these models employ beam-column elements with a fibre-based discretization of the section along the member's length. The modelling techniques associated with this approach are generally straightforward, since the model is constructed on basis of the cross-section geometry and uniaxial material properties. However, it lacks the ability to explicitly account for the interaction effects between parts (e.g. confinement stresses) as well as the development of

instability at the cross-section level (e.g. local buckling of the steel tube). This indicates that the DP model may be unsuitable for the predicting the flexural response of CFST member under cyclic loading, since these effects play a major role in the typical CFST response. To verify this assumption, specimen No.11 was modelled and analysed with the DP approach. In this research, a displacement-based beam-column element is adopted. Regarding the concrete and steel materials, the *OpenSees* [17] built-in uniaxial material model *steel02* and *concrete02* were adopted. The experimental and numerical responses of specimen No.11 are compared in Figure 5. As one may infer from the figure, the DP model fails to simulate strength deterioration. Moreover, the model cannot capture the concrete confinement effect by default, which will result in a conservative estimation of CFST's bending capacity.

3.1.2 Concentrated plasticity

The CP model is an alternative modelling approach that can be applied to CFST members. This model involves the consideration of rotational springs at the locations where plastic hinges are expected to occur. Thus, the model lumps the behaviour of the plastic hinge region into a nonlinear rotational spring, whilst the remaining portion of the element is assumed to remain elastic. As shown in Figure 4 (right), the model consists of one elastic beam-column element and one nonlinear rotational spring at each of the member's ends. The cyclic response of the CP model mainly depends on the hysteretic behaviour of the rotational spring. Therefore, it is necessary to adopt a suitable spring model to capture the cyclic flexural behaviour of the CFST member, especially in terms of deterioration and pinching effect.

Several researchers have developed rotational spring models for CFST members. The authors of [6] developed a hysteretic rule to represent the bending behaviour of circular CFST members. Similarly to the DP model, the proposed hysteretic rule has no strength deterioration features, and hence does not provide realistic member responses for circular CFSTs. Alternatively, other authors [15,19] have employed the modified Ibarra-Medina-Krawinkler deterioration model with peak-oriented hysteretic response (*ModIMKPeakOriented*) [16]. This model was originally proposed for reinforced concrete members, being able to capture strength and stiffness deterioration effects under cyclic loading. Differently from the DP model, building an accurate CP model requires reliable calibration data, which can accurately represent the seismic response of the member. Thus, a reliable calibration framework is required to calibrate the deterioration parameters to match the base response.

Figure 6 shows a comparison of moment-drift ratio curves between the test results and the calibrated CP model (Specimen No.3 and No.11, respectively). The calibration method described in [18] is used for calibration purposes to obtain the set of parameters of the *ModIMKPeakOriented* model. It can be seen that the elastic stiffness and the cyclic backbone curve of the target data are well simulated by the *ModIMKPeakOriented* model, which means that the simplified model should capture the cyclic strength deterioration of the CFST in a realistic manner. However, regarding each hysteretic cycle, the *ModIMKPeakOriented* model always predicts lower energy in comparison to the target data, which results in a conservative prediction of the dissipated energy. Thus, to directly apply the *ModIMKPeakOriented* model should lead to an inaccurate simulation of the cyclic flexural behaviour of CFST member.

3.2 Proposal of a new concentrated plasticity model for CFSTs

As discussed in the previous section, the available simplified numerical models have shortcomings in what concerns the simulation of strength deterioration effects and the hysteresis pattern of the behaviour (i.e. pinching effects). Thus, an accurate and efficient model for CFSTs, which can represent the cyclic behaviour of circular CFST member, is needed. As mentioned in Section 3.1.2, the CP model's response mainly depends on the hysteretic rules of its rotational spring model, which is customizable. Thus, a new rotational spring model, denoted as *matCFSTdet*, has been implemented in OpenSees [17]. The model was written C++ and has been compiled into a Dynamic-link library (DLL) file which can be linked to OpenSees model during run-time. Figure 7 shows the hysteretic loops of the *matCFSTdet* model together with its monotonic backbone curve. It is a Polygonal symmetrical hysteresis model with a tri-linear backbone curve.

3.2.1 Backbone curve

Figure 8 shows the monotonic backbone curve of the *matCFSTdet* model. To maintain consistency with the observation given in Section 2.2, the CFST's monotonic curve is simplified to a tri-linear shape. The CFST's elastic behaviour and plastic behaviour are simulated by the initial segment *OA* and the bilinear line *ABC*, respectively. Point *A* indicates that the member edge starts to yield whilst point *B* represents that the section is fully plastic. As discussed in Section 2.1, all specimens were observed to have little or no strength degradation occurring under monotonic loading. Thus, line *BC* of the backbone curve could be either set as ascending or as descending, which is different from the behaviour of *ModIMKPeakOriented* model. As marked in Figure 8, the *matCFSTdet* model's backbone curve is defined with 5 backbone parameters, namely the elastic stiffness (*K*), the yield moment

(M_1), the transition moment (M_2), the transition ratio (b_1) and the hardening ratio (b_2). The simplification procedures of the backbone curve are detailed in Section 4.1.

3.2.2 Hysteretic rules

When the cross-section is plastic and the load direction reverses, a new loading path will be created. The loading paths shown in Figure 9 are used to illustrate the *matCFSTdet* model's hysteretic rules. When unloading from point P_1, a new loading path $CP_1P_2P_3P_4$ is generated. The unloading stiffness at P_1 is $r_K K$, where r_K is a parameter to control the unloading stiffness deterioration under cyclic loading. The value of r_K depends on the accumulated rotation of the cross-section, which is detailed in Section 3.2.3. Point P_2 of is adopted as the intersection point of unloading path and the reverse line. As shown in Figure 9, if P_1 is at positive side, P_2 will be on the negative reverse line and vice versa. The absolute value of the reverse line is adopted as $r_R M_2$. The introduction of this reverse line aims to simulate the pinching effect. As discussed in Section 2.2, the severity of pinching effect relies on the loading history. Thus, the r_R parameter depends on the accumulated rotation, which is detailed in Section 3.2.3. Point P_3 is the corresponding point of P_1. Assuming that the coordinate at P_1 is (θ_p, M_p), then the coordinate at P_3 will be ($-\theta_p$, $-r_M M_p$), where r_M is the parameter to control the strength deterioration under cyclic loading, which is also detailed in Section 3.2.3.

In path $CP_1P_2P_3P_4$, only the unloading segment P_1P_2 represent the elastic stage of the cross-section. So reversing load direction at any other location will generate a new loading path. For example, as shown in Figure 9, when unloading from point Q_1 will update the loading path from $CP_1P_2P_3P_4$ to $P_4P_3Q_1Q_2Q_3Q_4$. The construction rule of points P_2 and P_3 also applies to the points Q_2 and Q_3.

3.2.3 Deterioration and pinching control

According to Section 2.2, not only strength deterioration but also the stiffness deterioration and pinching effect could significantly influence the hysteric response of circular CFST member. To simulate these effects, three parameters, namely r_M, r_K and r_R, are introduced to the *matCFSTdet* model. The parameter r_M, r_K and r_R control the strength deterioration, the stiffness deterioration, the pinching effect of the CFST cross-section under cyclic loading, respectively. Since the damage of the cross-section cumulates with the increase of loading cycle number, the normalized accumulated rotation (expressed in Equation (1), (2) and (3)) is adopted as the variable to indicate the CFST's damage level.

$$\theta'_{acc} = \frac{\theta_{acc}}{\theta_y} \quad (1)$$

$$\theta_y = \frac{M_1}{K} \quad (2)$$

$$\theta_{acc} = \sum_{i=2}^{N} |\theta_i - \theta_{i-1}| \quad (3)$$

where:

N is the current increment number;

θ'_{acc} is the normalized accumulated rotation of a given increment number N;

θ_{acc} is the accumulated rotation of a given increment number N;

θ_y is the yield rotation.

All three parameters (r_M, r_K and r_R) range from 0 to 1. The initial values of r_M, r_K equal to one, which means the strength/stiffness deteriorations have not occurred yet. The initial value of r_R is defined as R_{ini}, which represents the shape of the first hysteretic loop. The value of R_{ini} varies from different CFST cross-sections. With the increase of θ'_{acc}, the r_M, r_K and r_R will decrease to simulate the deterioration. It should be noted that the minimum values of three control parameters are limited to 10^{-5} to avoid convergence problems during analysing. For each parameter, two variables are introduced to control its degradation rate, as expressed in Equation (4) to (6). Thus, there are 7 parameters, namely R_{ini}, m_M, n_M, m_K, n_K, m_R and n_R, developed to control the deterioration and pinching effect, which is called control parameters in current research.

$$r_M = 1 - (m_M \theta'_{acc})^{n_M} \quad (4)$$

$$r_K = 1 - (m_K \theta'_{acc})^{n_K} \quad (5)$$

$$r_R = (1 - (m_R \theta'_{acc})^{n_R}) R_{ini} \quad (6)$$

where:

m_M and n_M are the parameters to control the strength deterioration;

m_K and n_K are the parameters to control the stiffness deterioration;

m_R and n_R are the parameters to control the pinching effect.

R_{ini} is the initial shape factor

4. Model calibration and verification

To build a concentrated plasticity model of a CFST member using the *matCFSTdet* model, 12 parameters (5 backbone parameters and 7 control parameters) are required. The calibration of these parameters relies on two target data (one monotonic data and one cyclic data). To confirm the accuracy of the model, the target data should represent the flexural response of circular CFST members precisely. The data could be obtained either from experimental tests or from

precise Finite Element model analysis which considers confinement effect, strength/stiffness deterioration and pinching effect. Besides the accurate target data, a proper calibration framework is also required so that the response of the calibrated *matCFSTdet* model can have a good agreement with the target data. In the following subsections, an advanced calibration framework, which aims to give an accurate and effective calibration to the *matCFSTdet* model, is described. The test results are used as target data to calibrate the model. The feasibility of the calibrated model is verified through a comparison of the results between the test and the Finite Element analysis.

4.1 Model calibration

The advanced calibration framework comprises two main steps, namely the monotonic backbone curve simplification and the control parameter calibration. The following two subsections detail the methods used in these steps, respectively.

4.1.1 Backbone parameters

To obtain the monotonic backbone curve of the *matCFSTdet* model, the monotonic target data needs to be simplified as a tri-linear curve. There are two types of monotonic backbone curve observed from test results. Figure 10 (a) shows the CFST member with a hardening behaviour at post-yield stage, which is mainly benefited from the concrete confinement effect. This curve type is referred as type A in the research. For specimens with degradation after the peak load (specimens No.6 and No.8), their monotonic backbone curve is defined as type B, which is shown in Figure 10 (b). The strength degradation is mainly due to a combined influence of axial load, steel tube local buckling effects and concrete crushing. Regarding the two backbone curve types, the simplification methods are slightly different. As shown in Figure 10 (a) and (b), three points (point *A*, point *B* and point *C*) which make up the tri-linear backbone curve are required to address. For both curve types, the last data point of the target data can be adopted as the point *C* of backbone. The elastic stiffness of the cross-section could be addressed as the slop of *OA'*. The point *A'* is defined as the point on target curve with a moment equals to $0.4M_{max}$, where M_{max} is the peak moment of target data. Regarding the acquirement of point *B*, different methods are applied to the two curves. For curve type A, point *B* is defined as the point which has a tangent slop equals to $0.1K$ whilst for curve type B, point *B* is addressed as the peak point of target curve. Finally, point *A* of backbone curve can be addressed on the extension line of *OA'*, in the way that the tri-linear curve has the same area with the target curve. With the tri-linear backbone curved addressed, the 5 backbone parameters (K, M_1, M_2, b_1 and b_2) can be adopted.

4.1.2 Control parameters

Differently from the backbone parameters, the control parameters (R_{ini}, m_M, n_M, m_K, n_K, m_R and n_R), which dominate the member's deterioration and the pinching effect, cannot be addressed from the target data directly. Thus, an accurate and efficient calibration method is developed for parameter acquirement purpose. A Genetic Algorithm (GA) [24], a powerful method to solve optimization problems, is utilized for the calibration of control parameters. The details of the calibration are described in the following.

Before calibration, the valid interval of each parameter is required. Theoretically, the 7 control parameters range from zero to infinity. But in order to reduce the calibration time, the parameter ranges should be narrowed. A preliminary calibration, which is based on trial and error, was conducted to narrow the parameter ranges, with intervals listed in Table 2.

Figure 11 illustrates the calibration procedures, which are based on the evolution of a *matCFSTdet* model group. The details of each calibration procedure are illustrated as follow:

Group Initialization: An initial group, which comprises 100 *matCFSTdet* models with randomly generated control parameters, are constructed.

Fitness Evaluation: The response of each model of the group is analysed under the loading history of target data. Based on the comparison between the target data and analytical results, the fitness of each model, expressed in Equation (7), can be evaluated. The fitness variable represents the accuracy of a given *matCFSTdet* model. A larger fitness value indicates a more accurate model.

Model Selection: The 100 models are sorted according to the fitness value in descending order. The top 60 models are selected and randomly paired.

Crossover: For each pair of models, the crossover process is performed to generate a pair of new *matCFSTdet* models. Specifically, the crossover is performed by creating two new copies of the paired models and exchanging the new models' first k control parameters, where k is a randomly generated integer from 1 to 6. Under this step, 60 new models are generated.

Mutation: Each parameter of the newly generated models has 10% of probability to be selected to mutate. The mutation of a parameter is performed by replacing its value by a randomly generated number (within the defined parameter range).

Fitness Evaluation: The fitness of the new generated *matCFSTdet* models are evaluated and sorted in descending order.

Elimination: The tail 60 *matCFSTdet* models of the group are eliminated from the group.

The procedures 3rd to 7th build up one evolution of the group. Finally, the group is evolved for 1000 times to achieve an accurate calibration. The *matCFSTdet* model which has the highest fitness of the group is adopted as the calibrated model corresponding to the target data.

$$fitness = \sqrt{\frac{N}{\sum_{i=1}^{N}\left(M_i^{FE} - M_i^{target}\right)^2}} \tag{7}$$

where:

N is total points number of the cyclic target data;

M_i^{target} is the moment of the i_{th} point from the cyclic target data;

M_i^{FE} is the moment of the i_{th} point from the Finite Element (FE) analysis.

4.2 Model validation

To validate the accuracy of the *matCFSTdet* model and the calibration framework, the tested specimens detailed in Section 2 were modelled and calibrated. It should be highlighted that the model is theoretically suitable for the simulation of CFSTs under both symmetric and asymmetric loading history flexure. However, since a symmetric loading history was considered during the experimental test, the model validation discussed in this section only refers to a symmetric loading history. Further studies should be conducted to validate this model for unsymmetrical loading history scenarios. As the rotation data of the CFST base cross-section was difficult to measure during the tests, the drift ratio was used to represent the member rotation. Since $\theta \approx tan\theta$ is true when θ is lower than 0.1, this assumption is deemed reasonable. It should also be highlighted that the data points recorded after steel fracture are not included during calibration as the model could not predict the occurrence of fracture in the steel tube.

Table 3 lists the 7 calibrated control parameters of each calibrated models together with their final fitness. Due to *i)* the limited number of specimens, *ii)* uncertainties related to the specimens (e.g., cross-section geometry, material properties, etc.) and to the test results (e.g. hysteretic loop asymmetry) and *iii)* randomness in the calibration procedure (e.g. group initialization, crossover and mutation), no clear relationship was observed between the control parameters and the characteristics of the specimens.

shows the moment versus drift ratio plots comparison between tests and Finite Element analysis. For specimens with significant asymmetry response (especially specimen No.9), the hysteretic loops of the calibrated model can only fit one side of the target curve as the model is proposed with symmetric backbone curve. As discussed in Section 2.2, the asymmetry of the member response is mainly caused by the asymmetric development of concrete cracking, which is unpredictable. Thus, the feasibility of the model and calibration framework is mainly evaluated based on results comparison of the specimens with relatively symmetric response. Overall, the accuracy of the *matCFSTdet* model is very good. It can be observed that with the employment of the *matCFSTdet* model and the calibration method, the unloading/reloading curves of the calibrated hysteretic loops are in good agreement with the target curves. For the cyclic specimens, the strength and stiffness deteriorations are accurately captured and the pinching effects are well simulated. Thus, it can be concluded that the CP approach with *matCFSTdet* model proposed in this work provides a high degree of accuracy for the simulation of CFST members under both monotonic and cyclic loading.

Table 4 summarizes the ultimate loads and total dissipated energy of the numerical and experimental results. M_{max}^{FE} and M_{min}^{FE} are the maximum and minimum bending moments from the Finite Element (FE) analysis, respectively. M_{max}^{test} and M_{min}^{test} are the maximum and minimum bending moments of the test results, respectively. The W_{FE} and W_{test} parameters represent the total dissipated energy values from the Finite Element (FE) analysis and the test results, respectively. The ultimate loads and total dissipated energy values are compared in terms of $\frac{M_{max}^{FE}}{M_{max}^{test}}$, $\frac{M_{min}^{FE}}{M_{min}^{test}}$ and $\frac{W_{FE}}{W_{test}}$. Assuming that a ratio lower than 10% is acceptable, the numerical ultimate moments are, generally, in good agreement with the experimental values, except for the M_{min}^{FE} values of 3 specimens (No.10, No.13 and No.15). The differences between the numerical and experimental values of the 3 specimens are mainly due to the asymmetry of the experimental hysteretic loops, since the model proposed herein is based on a symmetric backbone curve. It should be noted that, although the proposed model cannot capture the asymmetry of the hysteretic curves, it can keep a good balance between the maximum and minimum moments of the specimen as the average value of $\frac{M_{max}^{FE}}{M_{max}^{test}}$ and $\frac{M_{min}^{FE}}{M_{min}^{test}}$ is 94%. Moreover, despite the consideration of a symmetric backbone curve, the absolute values of M_{max}^{FE} and M_{min}^{FE} of each specimen are not equal. This is a result of the strength deterioration, which is

monotonically increasing during the loading history. Regarding the total dissipated energy, the W_{FE} values are on average 7% lower than the W_{test} values. This indicates that the calibrated models are able to capture the energy dissipation capability of the CFST members, which further verifies the feasibility of the proposed model. It should be noted that, as the proposed model is based on CP approach, it cannot consider the axial load-bending moment interaction, thus, different parameters are required for a CFST section under different axial load levels.

5. Conclusions

This paper focused on the proposal of a novel simplified numerical model for circular CFST members subjected to cyclic flexural loading. Based on experimental data, the flexural behaviour of circular CFST member was characterized. The feasibility of existing simplified modelling approaches was discussed. A novel approach, which represents the cross-section behaviour of circular CFST member, was developed and used as the nonlinear spring of the CP model. An accurate and efficient calibration framework has been proposed to find the optimum set of modelling parameters for the given target data. The accuracy of the calibrated model was verified through a comparison of the Finite Element results with the data obtained from the experimental tests. Based on the results obtained, the following conclusions can be extracted:

- Strength degradation, stiffness deterioration and pinching effects are observed from the hysteretic loops of circular CFST specimens, which are mainly caused by the concrete damage and steel local buckling under cyclic loading. The symmetry of the loops depends on the development of the concrete cracks, which is unpredictable.

- The DP model coupled with fibre cross-section fails to simulate the cyclic behaviour of CFST members, as it lacks the ability to capture the development of local buckling effects. The CP models from [15] and [18] are also not suitable for simulating the cyclic response of circular CFST since their hysteretic rules cannot accurately simulate the pinching effects.

- The developed *matCFSTdet* model, coupled with the proposed calibration method, reveals to be an efficient option for the simplified numerical simulation of the flexural response of circular CFST members. Strength deterioration, stiffness deterioration and pinching effects are well captured by the proposed model. It should be noted, however, that the model cannot capture the asymmetry of the cyclic response of CFST member as the asymmetry is mainly caused by unpredictable uncertainties related to the behaviour of CFST members.

ACKNOWLEDGMENTS

The authors wish to acknowledge the Portuguese Foundation for Science and Technology (FCT) for the financial support through the research project “Recycling & Seismic Protection: Sustainable High-Performance CFST Columns for Seismic Areas” (PTDC/ECM/117774/2010). Also acknowledged is the support of FERPINTA and PRESDOURO for providing test materials and preparing CFST specimens.

References

[1] L.-H. Han, Flexural behaviour of concrete-filled steel tubes, J. Constr. Steel Res. 60 (2004) 313–337.

[2] Z. Lai, A.H. Varma, Effective stress-strain relationships for analysis of noncompact and slender filled composite (CFT) members, Eng. Struct. 124 (2016) 457–472.

[3] S.B.B. Aval, M.A. Saadeghvaziri, A.A. Golafshani, Comprehensive composite inelastic fiber element for cyclic analysis of concrete-filled steel tube columns, J. Eng. Mech. 128 (2002) 428–437.

[4] E. Inai, A. Mukai, M. Kai, H. Tokinoya, T. Fukumoto, K. Mori, Behavior of concrete-filled steel tube beam columns, J. Struct. Eng. 130 (2004) 189–202.

[5] T. Fujimoto, A. Mukai, I. Nishiyama, K. Sakino, Behavior of eccentrically loaded concrete-filled steel tubular columns, J. Struct. Eng. 130 (2004) 203–212.

[6] L.-H. Han, Y.-F. Yang, Cyclic performance of concrete-filled steel CHS columns under flexural loading, J. Constr. Steel Res. 61 (2005) 423–452.

[7] A.H. Zubydan, A.I. ElSabbagh, Monotonic and cyclic behavior of concrete-filled steel-tube beam-columns considering local buckling effect, Thin-Walled Struct. 49 (2011) 465–481.

[8] C. Tort, J.F. Hajjar, Mixed finite-element modeling of rectangular concrete-filled steel tube members and frames under static and dynamic loads, J. Struct. Eng. 136 (2010) 654–664.

[9] K. Chung, J. Chung, S. Choi, Prediction of pre-and post-peak behavior of concrete-filled circular steel tube columns under cyclic loads using fiber element method, Thin-Walled Struct. 45 (2007) 747–758.

[10] B. Uy, Strength of concrete filled steel box columns incorporating local buckling, J. Struct. Eng. 126 (2000) 341–352.

[11] Q.Q. Liang, Performance-based analysis of concrete-filled steel tubular beam–columns, Part I: Theory and algorithms, J. Constr. Steel Res. 65 (2009) 363–372. doi:https://doi.org/10.1016/j.jcsr.2008.03.007.

[12] J.F. Hajjar, P.H. Schiller, A. Molodan, A distributed plasticity model for concrete-filled steel tube beam-columns with interlayer slip, Eng. Struct. 20 (1998) 663–676.

[13] M.D. Denavit, J.F. Hajjar, Nonlinear seismic analysis of circular concrete-filled steel tube members and frames, J. Struct. Eng. 138 (2011) 1089–1098.

[14] L.-H. Han, Y.-F. Yang, Z. Tao, Concrete-filled thin-walled steel SHS and RHS beam-columns subjected to cyclic loading, Thin-Walled Struct. 41 (2003) 801–833.

[15] C. Tucker, L. Ibarra, Effects of Partial-Design-Strength Concrete on the Seismic Performance of Concrete-Filled Tube Columns in Accelerated Bridge Construction, J. Bridg. Eng. 21 (2016) 4016023.

[16] D.G. Lignos, H. Krawinkler, Development and utilization of structural component databases for performance-based earthquake engineering, J. Struct. Eng. 139 (2012) 1382–1394.

[17] S. Mazzoni, F. McKenna, M.H. Scott, G.L. Fenves, The Open System for Earthquake Engineering Simulation (OpenSEES) User Command-Language Manual, (2006).

[18] A. Silva, Y. Jiang, L. Macedo, J.M. Castro, R. Monteiro, N. Silvestre, Seismic performance of composite moment-resisting frames achieved with sustainable CFST members, Front. Struct. Civ. Eng. 10 (2016). doi:10.1007/s11709-016-0345-y.

[19] A. Silva, Y. Jiang, J.M. Castro, N. Silvestre, R. Monteiro, Experimental assessment of the flexural behaviour of circular rubberized concrete-filled steel tubes, J. Constr. Steel Res. 122 (2016). doi:10.1016/j.jcsr.2016.04.016.

[20] H.R. Valipour, S.J. Foster, Nonlinear static and cyclic analysis of concrete-filled steel columns, J. Constr. Steel Res. 66 (2010) 793–802.

[21] S. Fan, L. Zhang, W. Sun, X. Ding, M. Liu, Numerical investigation on fire resistance of stainless steel columns with square hollow section under axial compression, Thin-Walled Struct. 98, Part A (2016) 185–195. doi:http://dx.doi.org/10.1016/j.tws.2015.09.010.

[22] L.-H. Han, H. Lu, G.-H. Yao, F.-Y. Liao, Further study on the flexural behaviour of concrete-filled steel tubes, J. Constr. Steel Res. 62 (2006) 554–565.

[23] A.K.H. Kwan, C.X. Dong, J.C.M. Ho, Axial and lateral stress–strain model for concrete-filled steel tubes, J. Constr. Steel Res. 122 (2016) 421–433.

[24] M. Mitchell, An introduction to genetic algorithms, MIT press, 1998.

Table 1 Specimens List

No.	Specimen Name	D [mm]	t [mm]	f_c [MPa]	f_y [MPa]	P [kN]	*Load Type*
1	CR-RuC15%-219-3-0%-M	219	2.8	20	309	0	Monotonic
2	CR-RuC15%-219-3-15%-M	219	2.8	20	309	222	Monotonic
3	CR-RuC15%-219-5-0%-M	219	4.7	20	393	0	Monotonic
4	CR-RuC15%-219-5-15%-M	219	4.7	20	393	290	Monotonic
5	CR-RuC5%-219-5-0%-M	219	4.7	39	393	0	Monotonic
6	CR-RuC5%-219-5-15%-M	219	4.7	39	393	359	Monotonic
7	CR-StdC-219-5-0%-M	219	4.7	53	393	0	Monotonic
8	CR-StdC-219-5-15%-M	219	4.7	53	393	393	Monotonic
9	CR-RuC15%-219-3-0%-C	219	2.8	20	309	0	Cyclic
10	CR-RuC15%-219-3-15%-C	219	2.8	20	309	222	Cyclic
11	CR-RuC15%-219-5-0%-C	219	4.7	20	393	0	Cyclic
12	CR-RuC15%-219-5-15%-C	219	4.7	20	393	290	Cyclic
13	CR-RuC5%-219-5-0%-C	219	4.7	39	393	0	Cyclic
14	CR-RuC5%-219-5-15%-C	219	4.7	39	393	359	Cyclic
15	CR-StdC-219-5-0%-C	219	4.7	53	393	0	Cyclic
16	CR-StdC-219-5-15%-C	219	4.7	53	393	393	Cyclic

where:

D is the external diameter;

t is the steel tube thickness;

f_c is concrete cube compressive strength;

f_y is the steel yield stress;

P is the constant axial load level.

Table 2 Narrowed ranges of the control parameters

Parameter name	Lower limit	Upper limit
R_{ini}	10^{-2}	1
m_M	10^{-5}	10^{-2}
m_K	10^{-5}	10^{-2}
m_R	10^{-5}	10^{-2}
n_M	10^{-1}	2
n_K	10^{-1}	2
n_R	10^{-1}	2

Table 3 Calibration results of the 8 specimens under cyclic loading

No.	Specimen Name	R_{ini}	m_M	m_K	m_R	n_M	n_K	n_R	Fitness
9	CR-RuC15%-219-3-0%-C	0.460	7.33×10^{-4}	1.39×10^{-3}	2.84×10^{-3}	0.55	0.72	1.22	0.151
10	CR-RuC15%-219-3-15%-C	0.974	4.45×10^{-6}	7.89×10^{-4}	3.01×10^{-3}	0.50	0.53	0.85	0.201
11	CR-RuC15%-219-5-0%-C	0.591	1.58×10^{-3}	9.16×10^{-4}	1.55×10^{-3}	1.50	0.51	1.49	0.194
12	CR-RuC15%-219-5-15%-C	0.514	1.29×10^{-4}	9.53×10^{-4}	2.07×10^{-4}	0.77	1.50	0.79	0.114
13	CR-RuC5%-219-5-0%-C	0.559	2.02×10^{-3}	1.15×10^{-3}	1.88×10^{-3}	1.50	0.62	1.48	0.173
14	CR-RuC5%-219-5-15%-C	0.506	9.28×10^{-5}	1.04×10^{-3}	2.77×10^{-5}	0.65	0.50	1.50	0.092
15	CR-StdC-219-5-0%-C	0.601	1.39×10^{-3}	1.05×10^{-3}	1.22×10^{-3}	1.20	0.61	1.06	0.157
16	CR-StdC-219-5-15%-C	0.476	8.09×10^{-4}	1.04×10^{-3}	2.25×10^{-6}	1.48	0.50	1.50	0.101

Table 4 Ultimate loads and total dissipated energy comparisons between numerical prediction and test results

No.	Specimen Name	M_{max}^{FE} [kNm]	M_{min}^{FE} [kNm]	W_{FE} [kNm]	M_{max}^{test} [kNm]	M_{min}^{test} [kNm]	W_{test} [kNm]	$\frac{M_{max}^{FE}}{M_{max}^{test}}$	$\frac{M_{min}^{FE}}{M_{min}^{test}}$	$\frac{W_{FE}}{W_{test}}$
9	CR-RuC15%-219-3-0%-C	59	-50	55	63	-46	55	93%	108%	98%
10	CR-RuC15%-219-3-15%-C	71	-71	31	74	-90	35	95%	79%	90%
11	CR-RuC15%-219-5-0%-C	104	-104	158	108	-115	165	97%	90%	96%
12	CR-RuC15%-219-5-15%-C	131	-130	53	130	-142	63	101%	91%	85%
13	CR-RuC5%-219-5-0%-C	111	-107	144	114	-121	148	97%	88%	97%
14	CR-RuC5%-219-5-15%-C	130	-125	52	137	-139	58	95%	90%	88%
15	CR-StdC-219-5-0%-C	111	-108	141	113	-130	145	98%	83%	97%
16	CR-StdC-219-5-15%-C	134	-134	53	133	-146	59	100%	92%	89%
							Average:	94%		93%

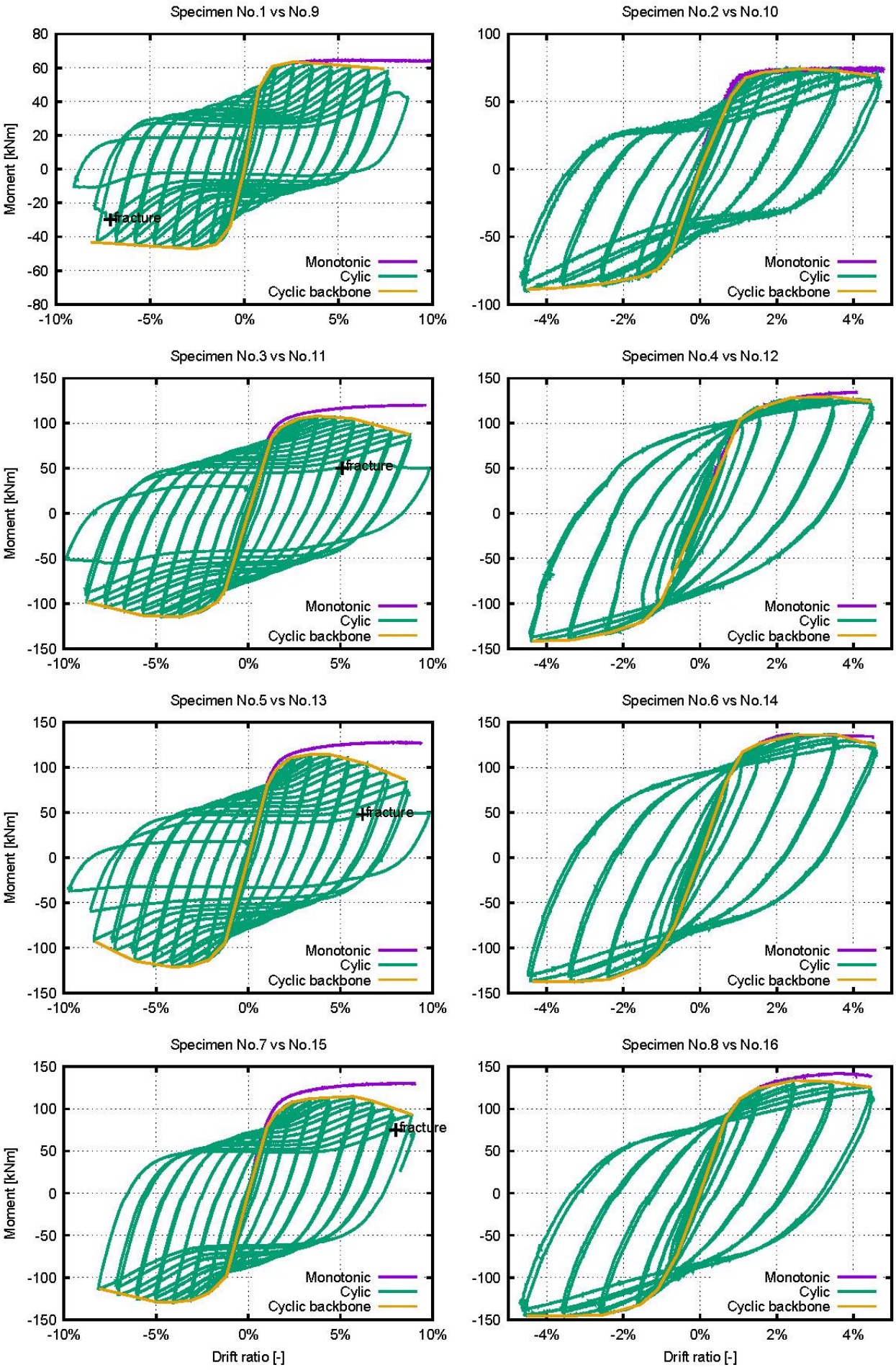

Figure 1 Moment-drift ratio plots of the 16 circular CFST specimens

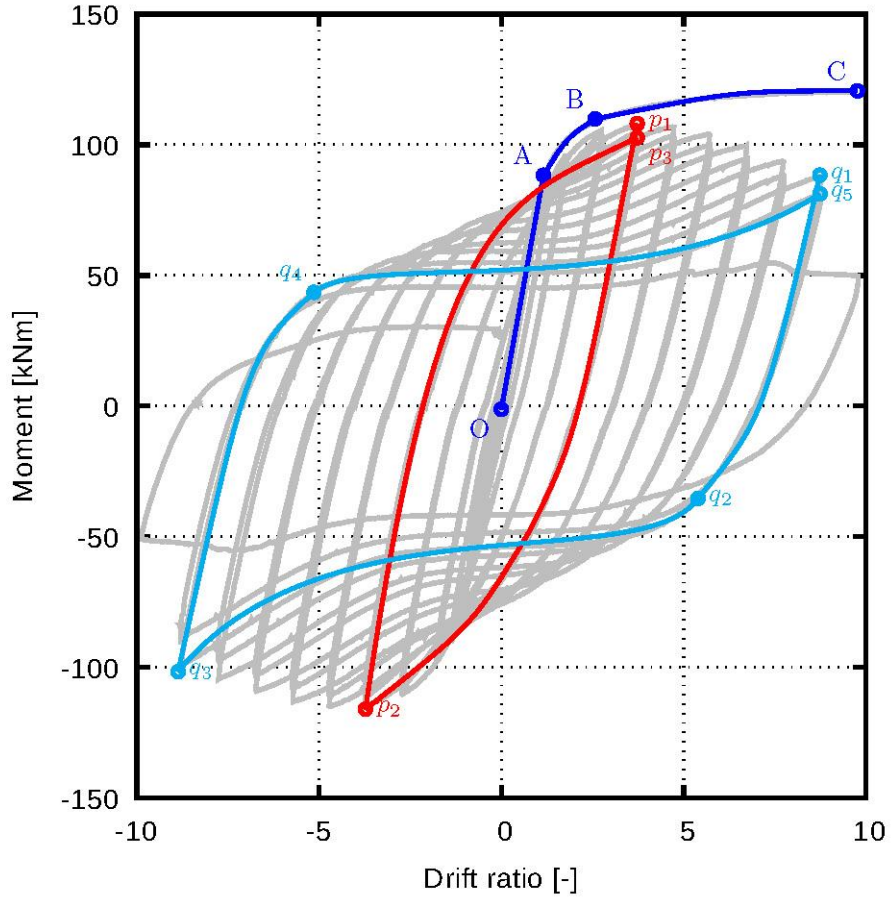

Figure 2 Flexural behaviour of specimens No.3 (monotonic) and No.11 (cyclic)

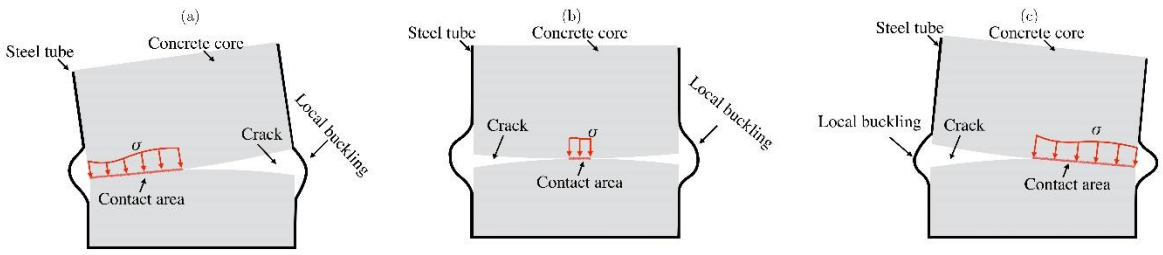

Figure 3 Concrete cracking of circular CFST under large deformation

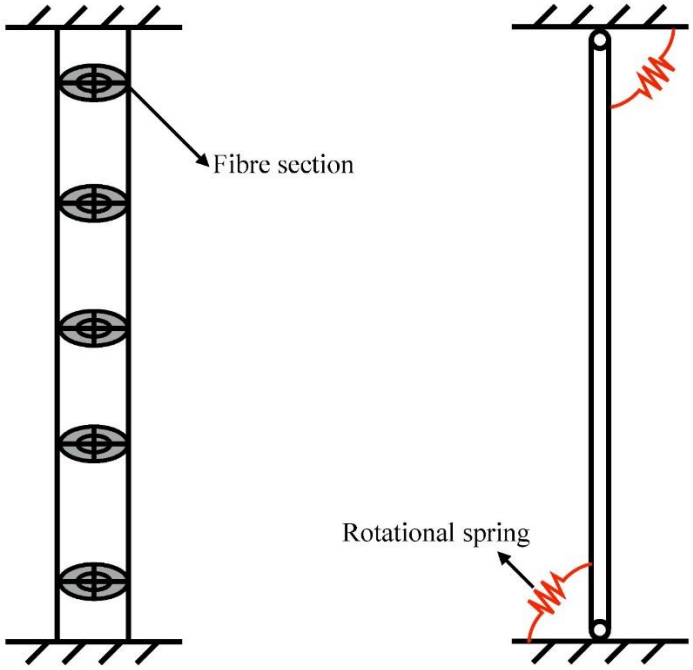

Figure 4 Distributed Plasticity (left) and Concentrated Plasticity (right) models

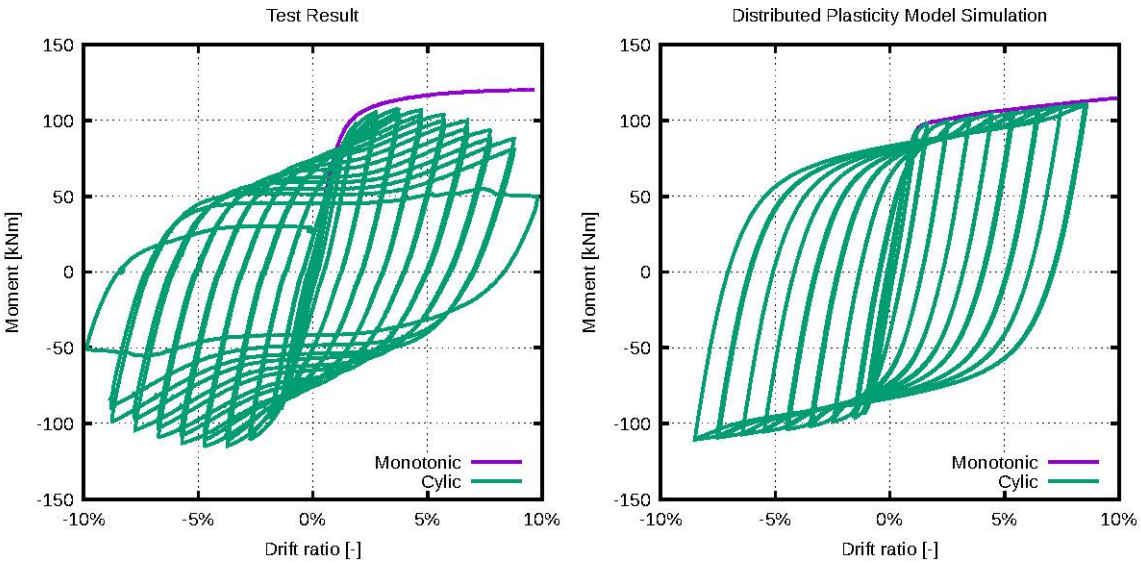

Figure 5 Comparison of moment-drift ratio plots between the test results and DP model prediction (Specimen No.3 and No.11)

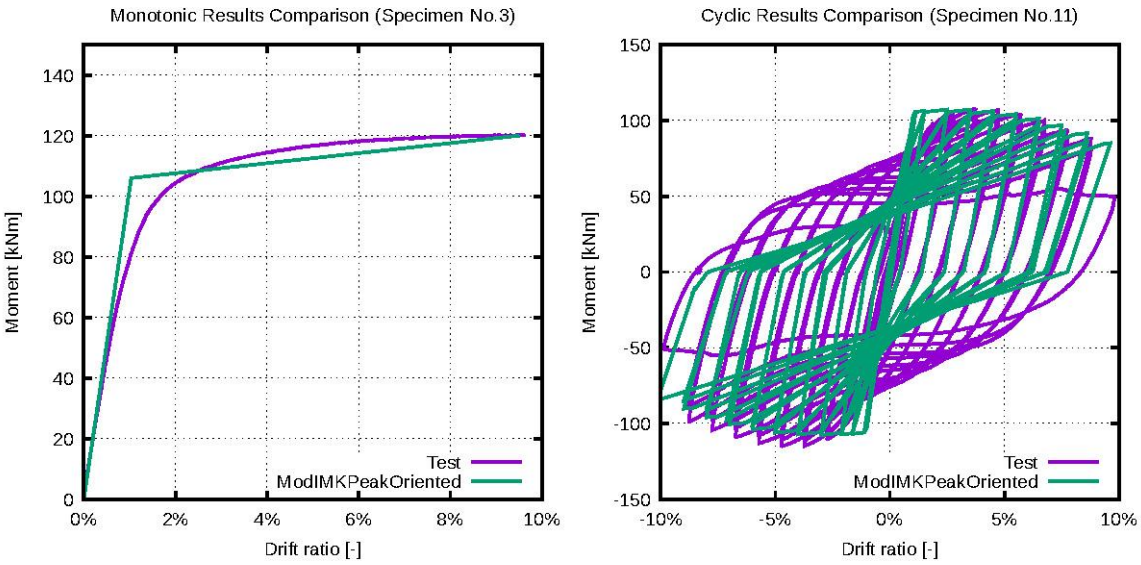

Figure 6 Comparison of moment-drift ratio plots between the test results and Concentrated Plasticity model (with *ModIMKPeakOriented*) prediction

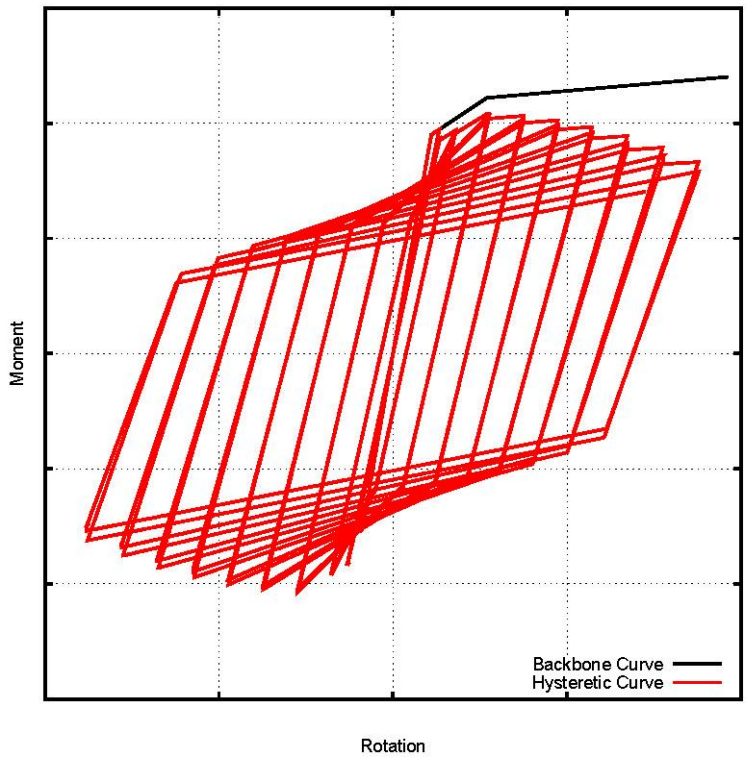

Figure 7 Hysteretic loops of the *matCFSTdet* Model

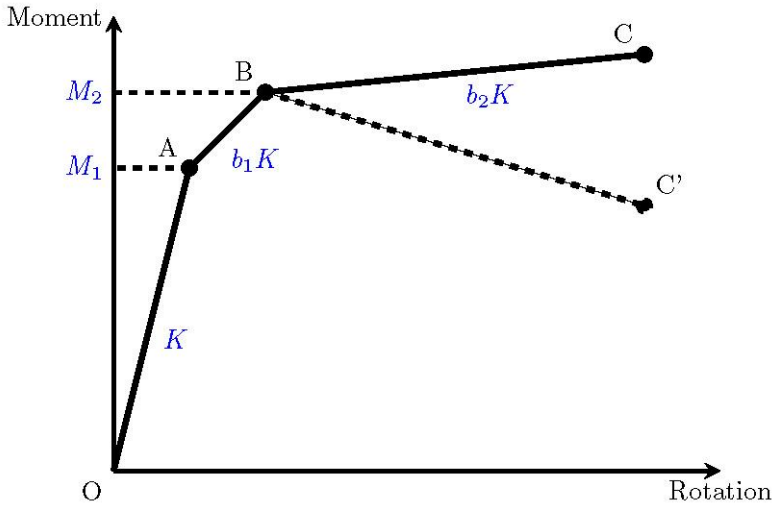

Figure 8 Monotonic backbone curve of *matCFSTdet* Model and its five backbone parameters

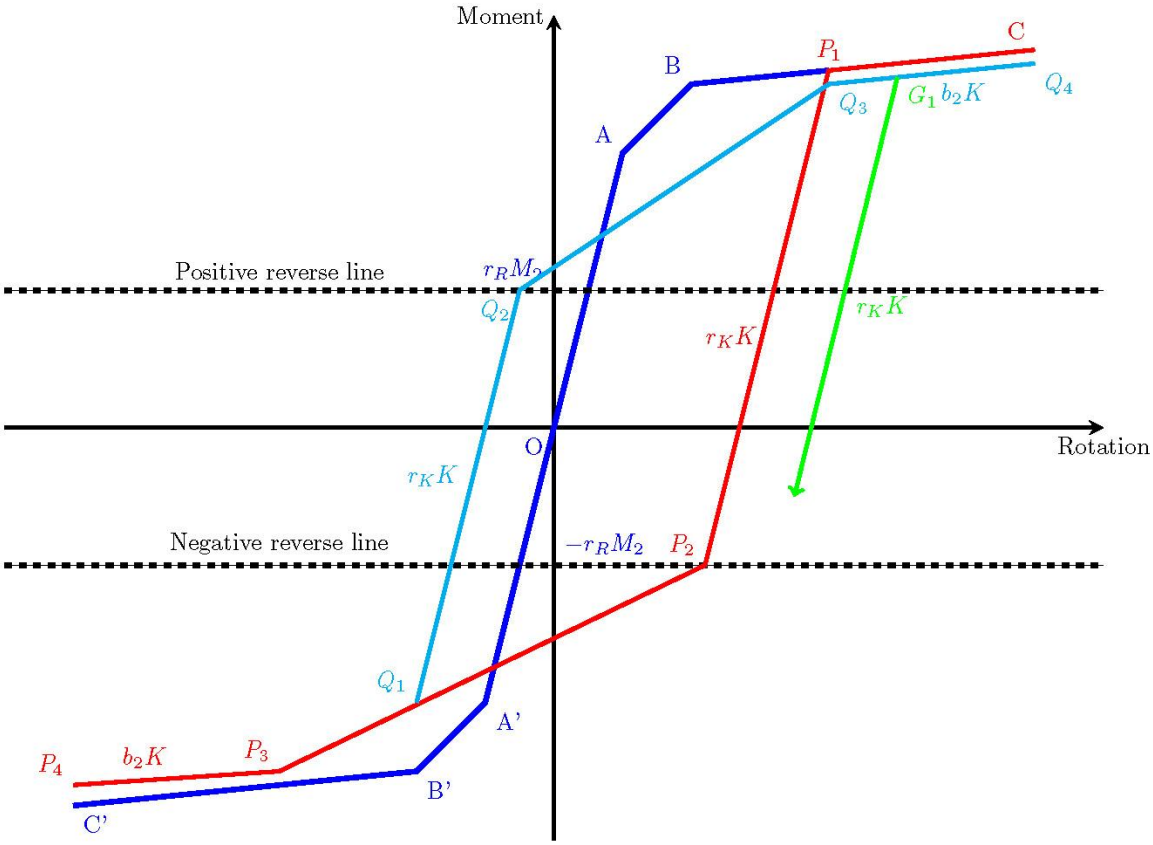

Figure 9 Unloading/reloading rule of the *matCFSTdet* model

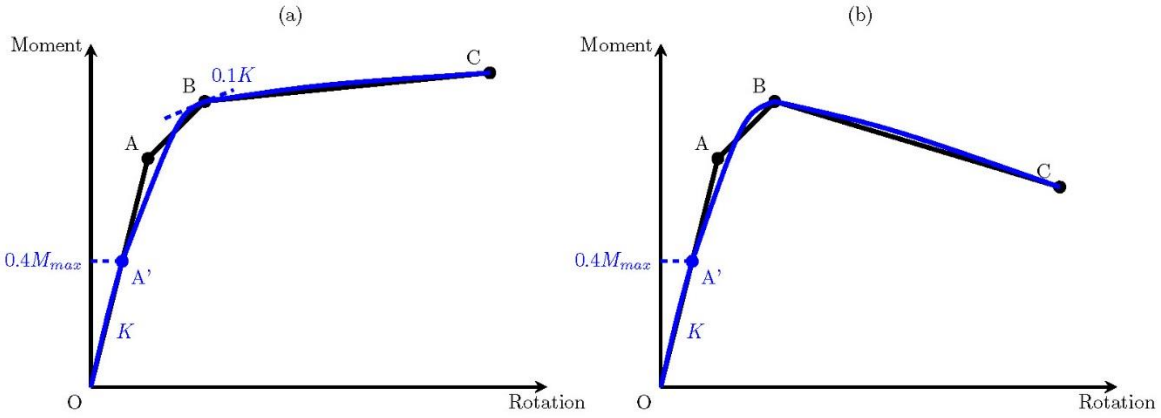

Figure 10 Monotonic backbone curve simplification (a) for curve type A and (b) for curve type B

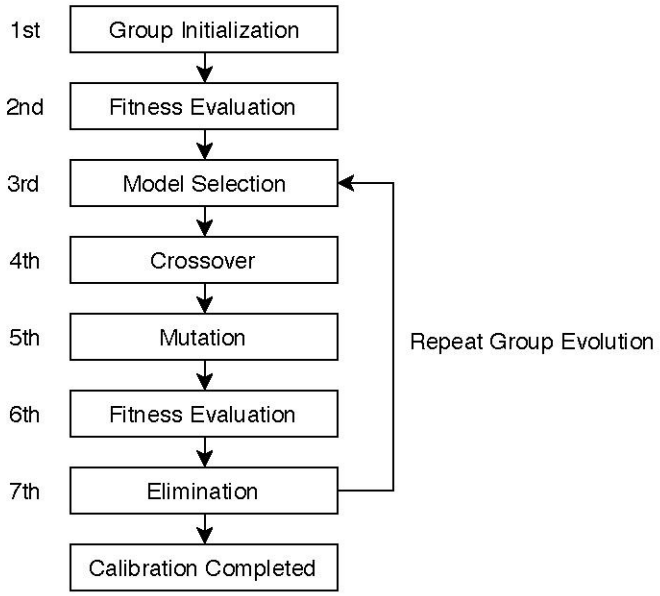

Figure 11 Calibration procedures based on Genetic Algorithm

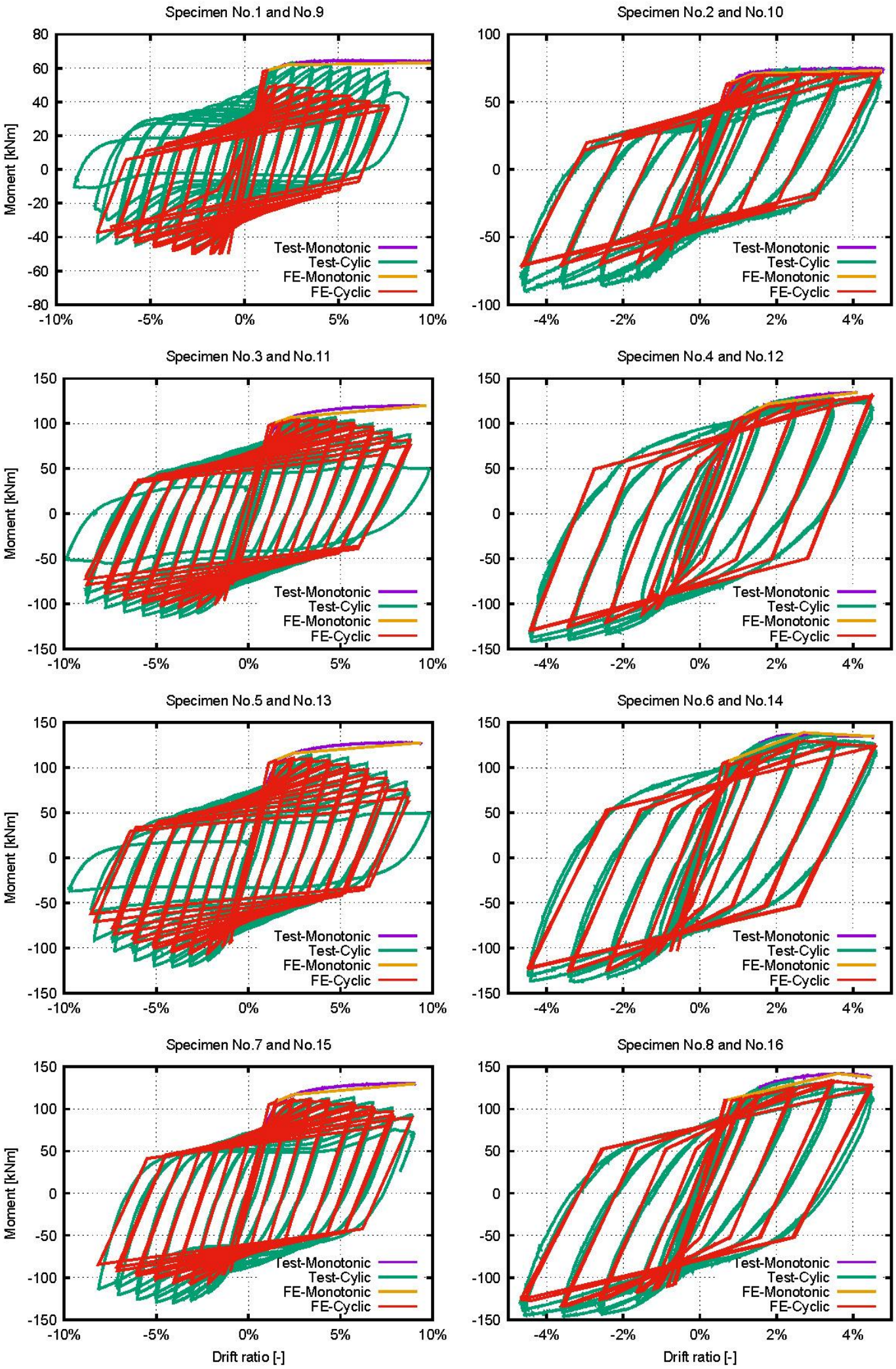

Figure 12 Comparison of moment-drift ratio plots between test results and Concentrated Plasticity model (with *matCFSTdet*) prediction